Published in final edited form as:
Neuroscience. 2009 July 21; 161(4): 1091–1103. doi:10.1016/j.neuroscience.2009.04.024.

Spatial and intracellular relationships between the α7 nicotinic acetylcholine receptor and the vesicular acetylcholine transporter in the prefrontal cortex of rat and mouse

Aine M. Duffy, **Ping Zhou**, **Teresa A. Milner**, and **Virginia M. Pickel***
Division of Neurobiology, Department of Neurology and Neuroscience, Weill Cornell Medical College, 411 East 69th Street, New York, NY 10021, USA

Abstract

The alpha-7 subunit of the nicotinic acetylcholine receptor (α7nAChR) is expressed in the prefrontal cortex (PFC), a brain region where these receptors are implicated in cognitive function and in the pathophysiology of schizophrenia. Activation of this receptor is dependent on release of acetylcholine (ACh) from axon terminals that contain the vesicular acetylcholine transporter (VAChT). Since rat and mouse models are widely used for studies of specific abnormalities in schizophrenia, we sought to determine the subcellular location of the α7nAChR with respect to VAChT storage vesicles in axon terminals in the PFC in both species. For this, we used dual electron microscopic immunogold and immunoperoxidase labeling of antisera raised against the α7nAChR and VAChT. In both species, the α7nAChR-immunoreactivity (-ir) was principally identified within dendrites and dendritic spines, receptive to axon terminals forming asymmetric excitatory-type synapses, but lacking detectable α7nAChR or VAChT-ir.

Quantitative analysis of the rat PFC revealed that of α7nAChR labeled neuronal profiles, 65% (299/463) were postsynaptic structures (dendrites and dendritic spine) and only 22% (104/463) were axon terminals or small unmyelinated axons. In contrast, VAChT was principally localized to varicose vesicle-filled axonal profiles, without recognized synaptic specializations (n = 240). Of the α7nAChR-labeled axons, 47% (37/79) also contained VAChT, suggesting that ACh release is autoregulated through the presynaptic α7nAChR. The VAChT-labeled terminals rarely formed synapses, but frequently apposed α7nAChR-containing neuronal profiles. These results suggest that in rodent PFC, the α7nAChR plays a major role in modulation of the postsynaptic excitation in spiny dendrites in contact with VAChT containing axons.

Keywords

autoregulation; cognitive function; cholinergic; immunocytochemistry; electron microscopy; schizophrenia

*Address correspondence to: Dr. Virginia M. Pickel, Division of Neurobiology, Weill Cornell Medical College, 411 East 69th Street, New York, NY 10021, Phone: (212) 570-2900, FAX: (212) 988-3672, email: E-mail: vpickel@med.cornell.edu.
Section Editor: Dr. Charles R. Gerfen

Introduction

Abnormalities in the function of the α7nAChR and cholinergic transmission in the PFC are implicated in the cognitive deficits seen in schizophrenia (Severance and Yolken, 2008). Moreover, polymorphic variations of the CHRNA7 gene, which encodes the α7nAChR, are linked to schizophrenia (Leonard et al., 2002, Freedman et al., 2006), especially the notable auditory gating deficits seen in schizophrenic patients (Freedman et al., 1997, Gault et al., 2003). Agonists of the α7nAChR normalize these gating deficits in animal models of schizophrenia (O'Neill et al., 2003, Martin et al., 2004). In addition, α7nAChR binding is reduced in the frontal cortex of post-mortem samples from schizophrenic patients further implicating cortical α7nAChR in schizophrenia (Guan et al., 1999, Marutle et al., 2001, Martin-Ruiz et al., 2003, Severance and Yolken, 2008).

Although previous light and electron microscopic studies have shown that the α7nAChR is expressed in the PFC (Dominguez del Toro et al., 1994, Lubin et al., 1999), the critical location of the α7nAChR relative to the endogenous ligand, acetylcholine (ACh) is not known. PFC ACh is derived primarily from cholinergic inputs to deep layers (III-VI) from the basal forebrain (Lehmann et al., 1980, Gaykema et al., 1990, Woolf, 1991, Butcher, 1995, Zaborszky et al., 1997, Henny and Jones, 2008). These cholinergic terminals represent only a small fraction of all cortical synapses (Descarries and Mechawar, 2000). This observation together with microdialysis studies showing a comparatively large volume of cortically released ACh led to the hypothesis by Descarries (1997) that ACh exerts its effects *via* diffusion or volume transmission. Thus, the released ACh may non-synaptically activate the α7nAChR within neurons located a short-range distance from an ACh-containing axon terminal. This suggests that a single ACh-containing terminal may influence α7nACh receptors located at multiple sites. Such global actions could profoundly affect microdomains within the PFC that have relevance to cognitive functions impaired in schizophrenia.

To address the key question of the location of the α7nAChR with respect to it's endogenous ligand ACh in the PFC, we examined the electron microscopic immunolabeling of the α7nAChR and VAChT in single sections through the PFC of rat and mouse. These two species were chosen because of their extensive use as either pharmacological (rat) or genetic (mouse) models of the somatosensory gating deficits that are typical of schizophrenia (O'Neill et al., 2003, Duncan et al., 2004).

Our results define the subcellular location of the α7nAChR with respect to neuronal compartments, and their spatial or intracellular relationship to VAChT-containing axonal profiles without recognizable synaptic specializations in the PFC of both species. Shown here, the PFC α7nAChR is specifically targeted to postsynaptic dendritic spines apposed to or within the critical diffusion space (0.2 μm) from VAChT-labeled axon terminals almost half of which express the α7nAChR.

Experimental Procedures

Animals

The experimental procedures were carried out in accordance with the National Institutes of *Health Guidelines for the Care and Use of Laboratory Animals*, and approved by the Institutional Animal Care and Use Committees (IACUC) at Weill-Cornell Medical College. Twelve male Sprague-Dawley rats (180–200 g; Charles River, Kingston NY) and 12 male C57BL/6J mice (20–25 g; Charles River, Kingston NY) were deeply anesthetized by intraperitoneal (*i.p.*) injection of sodium pentobarbital (100 mg/kg). For Western blot analysis, both rats and mice (n = 3) were decapitated, and the brain was rapidly removed for lysate

preparation. The other animals (n = 9) were fixed by vascular perfusion with an aldehyde solution in preparation for microscopic analysis.

Antisera

A commercial polyclonal VAChT antiserum (Chemicon, Temecula, CA, U.S.A.) was used to identify cholinergic processes in the PFC. This antiserum was raised in goat against a synthetic peptide corresponding to amino acids 511-530 from cloned rat VAChT (Erickson et al., 1994, Roghani et al., 1994). Studies have been performed previously to characterize the antiserum, which selectively labels CV-1 cells transfected with VAChT cDNA (Arvidsson et al., 1997). This antiserum shows a specific band at the predicted 70 kDa molecular weight in Western blots of tissue (Brunelli et al., 2005). The VAChT antiserum has been used extensively in electron microscopy studies in the rat to identify cholinergic processes (Garzón and Pickel, 2000, Pickel et al., 2000, Svingos et al., 2001, Towart et al., 2003, Kaplan et al., 2004).

A mouse monoclonal anti-α7nAChR antibody (clone mAb306; Sigma, St. Louis, MO, U.S.A.) was generated using affinity–purified native chicken and rat α-bungarotoxin binding proteins (Schoepfer et al., 1990). Epitope mapping has shown that mAb306 recognizes the sequence corresponding to the cytoplasmic loop residues 380-400 of the α7nAChR from rat and chicken (Schoepfer et al., 1990, McLane et al., 1992). This antibody was used previously to study the α7nAChR distribution, in (1) rat brain using bright field (Dominguez del Toro et al., 1994), or electron microscopy (Fabian-Fine et al., 2001, Levy and Aoki, 2002) and (2) macaque brain using fluorescent microscopy (Centeno et al., 2006). Since, the α7nAChR antibody had not previously been examined in Western blotting of cerebral cortex, we performed the analysis in rat and mouse as a means of further characterization. In addition sections were processed for light microscopic analysis of α7nAChR or VAChT in the presence of 0.25% Triton X-100 for establishing the optimal dilution of each antisera.

Western Blot

Total protein lysates of rat and mouse cerebral cortex were prepared on ice. Tissues were solubilized in cell lysis buffer [20 mM Tris-saline (TS) pH 7.5, 150 mM NaCl, 1 mM EDTA, 1 mM EGTA, 1% Triton X-100, 2.5 mM sodium pyrophosphate, 1 mM beta-glycerolphosphate, 1 mM Na_3VO_4, 1 μg/ml leupeptin]. The protein concentration of the lysates were determined with the protein assay reagent (Bio-Rad, Hercules, CA, U.S.A.). Samples were boiled for 5 minutes in SDS loading buffer before 30 μg (rat) and 100 μg (mouse) of samples were loaded directly onto a 12% SDS-polyacrylamide gel, along with molecular weight markers (Kalidescope; Bio-Rad). Proteins were transferred to a PVDF nylon membrane (Millipore, Billerica, MA, U.S.A), and the membrane was blocked in 5% nonfat dry milk (Nestle Food Company, Glendale, CA, U.S.A) in 100 mM Tris-buffered saline and 0.1% Tween-20 (TBST/T; Bio-Rad) for 60 minutes. The membranes were incubated with the α7nAChR antibody at a dilution of 1:1,000 at 4°C for 3 days. The blots were rinsed in TBST/T and incubated at room temperature for 60 minutes with goat anti-mouse immunoglobulin (IgG) conjugated with horseradish peroxidase (Jackson Immunoresearch Laboratories, West Grove, PA, U.S.A) at a dilution of 1:2,000 in 5% nonfat milk. The blot was developed using the Supersignal substrate reagents (Pierce, Rockford, IL, U.S.A), and the images were captured on a Kodak image station (Eastman Kodak, Rochester, NY, U.S.A).

Fixation and tissue preparation

Brain tissue was aldehyde fixed for immunolabeling by perfusion through the ascending aorta (rat) or the left ventricle of the heart (mouse). This was achieved using a Masterflex pump (Barnat Company, Barrington, IL, U.S.A) to rapidly (<5 minutes) and sequentially deliver solutions of (1) normal saline (0.9%) containing 1000 units/ml of heparin (10–15 ml), (2) 40–50 ml of 0.1 M phosphate buffer (PB; pH 7.4) containing 3.75% acrolein and 2%

paraformaldehyde, and (3) 250 ml of 2% paraformaldehyde in PB. The brains were then removed from the cranium, cut into 4–5 mm coronal blocks and post-fixed for 30 minutes in the latter fixative.

Coronal sections (40 μm thick) were cut through the PFC using a Leica Vibratome (Leica Microsystems, Bannockburn, IL, U.S.A.). Sections through the PFC corresponded to +2.8 mm from Bregma in rat (Paxinos and Watson, 1986) and +2.2 mm from Bregma in mouse (Paxinos and Franklin, 2001). Rat and mouse sections were processed for light and electron microscopy together. Firstly, sections were placed for 30 minutes in a solution of 1% sodium borohydride in 0.1 M PB to remove excess active aldehydes. These were rinsed in 0.1 M PB and incubated for 15 minutes in a cryoprotectant solution (25% sucrose and 3% glycerol in 0.05 M PB) prior to freeze-thawing to enhance penetration of immunoreagents. The cryoprotected sections were sequentially immersed in liquid chlorodifluoromethane (Freon, Blasco Supply, Bronx, NY) and liquid nitrogen, then thawed by immersion in 0.1 M PB. After extensive rinsing in 0.1 M TS (pH 7.6), the sections were incubated for 30 minutes in 0.5% bovine serum albumin (BSA) in 0.1 M TS to minimize non-specific attachment of anitsera or immunoreagents during the process of immunolabeling.

Immunolabeling

PFC sections from rat and mouse were processed for single-immunoperoxidase and dual-immunoperoxidase/immunogold labeling of α7nAChR and VAChT (Chan et al., 1990, Hara and Pickel, 2008, Lane et al., 2008). The primary antisera against α7nAChR and VAChT were raised in mouse and goat, respectively, and therefore could be recognized in a single section by appropriate species-specific secondary antibodies.

Sections for single-immunoperoxidase were incubated in a solution of 0.1% BSA in TS, containing mouse monoclonal antibody for α7nAChR diluted 1:1,000 or the goat polyclonal antiserum for VAChT diluted 1:8,000. The sections were incubated for 24 hours at room temperature and 24 hours at 4°C for VAChT-labeled sections, with a further 48 hour incubation for α7nAChR labeled sections. For dual immunoperoxidase/immunogold labeling, sections were incubated in a solution of 0.1% BAS in TS, containing mouse monoclonal antibody for α7nAChR diluted 1:500 for 24 hours at room temperature and 24 hours at 4°C. The goat polyclonal antiserum for VAChT (1:8,000) was added and the incubation continued for 48 hours at 4°C. After incubation in these primary antisera, the sections were first processed for either (A) single immunoperoxidase labeling only or (B) immunoperoxidase and followed by immunogold labeling. All the incubations were carried out at room temperature with continuous agitation on a rotator, and were followed by several rinses in the appropriate buffer.

For the immunoperoxidase visualization of antigens, the avidin-biotin complex (ABC) method (Hsu et al., 1981) was used. Incubation in primary antisera was followed by incubation in secondary biotinylated antibody (1:400; horse anti-mouse IgG for α7nAChR; Jackson; or donkey anti-goat IgG for VAChT; Jackson) for 30 minutes and then in ABC (1:100; Vectastain Elite Kit; Vector Laboratories) for 30 minutes. The immunoreactivity bound to the tissue was visualized by a 6-minute incubation in 0.022% 3,3-diaminobenzidine (DAB) and 0.003% hydrogen peroxide in 0.1 M TS, pH 7.6.

The sections for dual immunoperoxidase/immunogold labeling were then processedfor silver-enhanced immunogold labeling (Chan et al., 1990). For this, the sections were rinsed in 0.1 M TS, transferred to 0.01 M phosphate buffered saline (PBS), blocked for 10 minutes in 0.8% BSA and 0.1% gelatin in 0.01 M PBS, and incubated for 2 hours in colloidal gold (1 nm)-labeled IgG (1:50; donkey anti-mouse IgG for α7nAChR; or donkey anti-goat IgG for VAChT; Electron Microscopy Sciences, Fort Washington, PA, U.S.A.). After this, the sections were

fixed for 10 minutes in 2% glutaraldehyde in 0.01 M PBS and reacted with a silver solution IntenSEM kit (Amersham) for 7 minutes.

For quantification, the immunogold-silver method was used for detection of α7nAChR and immunoperoxidase detection of VAChT. However, the markers were reversed in a few sections to ensure maximal detection of each antisera as there are known differences in sensitivity for each method (Chan et al., 1990). In addition, sections were processed for both immunogold and immunoperoxidase α7nAChR and VAChT alone, to obtain optimal dilutions of each primary antiserum. As a control for non-specific labeling, sections were processed for immunoperoxidase and immunogold labeling, omitting each of the primary antisera.

Electron microscopic tissue processing and data analysis

Immunolabeled PFC sections used for electron microscopy were postfixed in 2% osmium tetroxide in 0.1 M PB for 1 hour. These sections then were dehydrated through a series of graded ethanols to propylene oxide, and embedded in Epon (EMbed-812; Electron Microscopy Sciences) between two sheets of Aclar plastic (Allied Signal, Pottsville, PA, U.S.A.). The flat-embedded plastic sections were glued on Epon chucks, trimmed to ~1 mm pyramids in middle-deep PFC layers. Ultrathin sections (65 – 75 nm thick) were cut from the tissue-Epon interface with a diamond knife (Diatome, Fort Washington, PA, U.S.A.) on an ultramicrotome (Leica Microsystems, Bannockburn, IL, U.S.A.). Ultrathin sections from PFC layer III–V were collected on 400-mesh copper grids (Fig. 1), counterstained with uranyl acetate and Reynold's lead citrate (Reynolds, 1963), and examined with a Phillips CM10 electron microscope.

Images were collected only from ultrathin sections near the plastic-tissue interface (*i.e.* surface of the tissue) to reduce false negatives resulting from inadequate penetration of antisera. The classification of identified cellular elements was based on the descriptions of Peters *et al*. (1991). Axon terminals were identified by the presence of numerous synaptic vesicles and were at least 0.2 μm in diameter. Small, unmyelinated axons were <0.1 μm and rarely contained small vesicles. Neuronal somata were identified by the presence of a nucleus, Golgi apparatus, and rough endoplasmic reticulum. Dendrites were postsynaptic to axon terminals, contained abundant endoplasmic reticulum, and few, if any small vesicles. Most dendrites were >0.1 μm in cross-sectional diameter. Glial processes were identified by their irregular shape, which followed the contours of neuronal profiles. The glial cytoplasm also often contained bundles of filaments. Asymmetric synapses were recognized by thick postsynaptic densities, whereas symmetric synapses had thin pre- and postsynaptic specializations. Zones of closely spaced parallel plasma membranes, without discernible synaptic densities or glial interventions, were defined as appositions or nonsynaptic contacts. A profile was considered to be selectively immunoperoxidase labeled when it contained electron dense cytoplasmic precipitates not seen in morphologically similar profiles located within the surrounding neuropil. Large profiles >0.5 μm were considered immunogold labeled when they contained two or more gold particles. In dendrites <0.5 μm diameter and in small, unmyelinated axons (<0.5 μm diameter), a single particle was considered positive for immunogold labeling. The validity of this approach was established by the absence of gold-silver deposits over myelin and other tissue elements not known to express the α7nAChR, an approach that has previously been used for immunolabeling of other receptor proteins (Garzón and Pickel, 2006). In addition, however we examined the number of gold particles over dendritic and axonal profiles in control experiments in which the tissue was processed for dual labeling with the omission of one of the respective primary antisera to assess the level of background spurious gold-silver particles. In dendrites of all sizes, the particles were considered extrasynaptic when located >50 nm away from the edge of the nearest synapse, while those within the soma radius were considered perisynaptic.

Electron microscopic images were taken from thin sections collected from the middle layers of the PFC in vibratome sections processed for α7nAChR-immunoperoxidase or α7nAChR-

immunogold and VAChT-immunoperoxidase labeling. At least three immunolabeled vibratome sections from each animal was included in the quantitative (rat) and qualitative (mouse) analysis All immunoreactive processes (n = 770) were counted in randomly sampled electron micrographs at x13,500–34,000 from an area of 17,989μm^2. For analysis of the number of VAChT- compared to α7nAChR-labeled neuronal profiles in an electron microscopic grid square corresponding to an area of 54 μm^2, the entire field was photographed in each rat (n = 4).

The tissue was quantitatively examined to determine the relative frequencies with which the immunoreactive products were localized within neuronal somata, dendrites, axons, and glial profiles. In addition, each α7nAChR-labeled neuronal profile was defined with respect to appositional contacts and distance from nearest VAChT-labeled axon. One-way analysis of variance (ANOVA) was performed using SPSS (SPSS Inc., Chicago, IL, USA) to ensure that there was no significant inter-animal variability in the number of immunoreactive α7nAChR-labeled profiles or VAChT-labeled axons. MCID Elite software (version 6.0, Imaging Research Inc., St. Catharines, ON, Canada) was used to measure the shortest distance between α7nAChR- and VAChT-labeled profiles.

Light Microscopic Analysis

For light microscopy the immunoperoxidase labeled sections were rinsed in 0.05 M PB, and mounted on gelatin-coated glass slides. After overnight drying in a dessicator, the sections were dehydrated by sequential immersion in a series of increasing-concentrations of alcohol and defatted in xylene (J.T. Baker, Phillipsburg, NJ, U.S.A.). The slides were then coverslipped with Permount (Fisher Scientific, Fair Lawn, NJ, U.S.A.)

Image Analysis

The electron microscopic images used for the analysis and figures were acquired with an AMT digital camera (Advanced Microscopy Techniques Corporation, Danvers, MA) on a Microsmart computer with a Windows, 2000 operating system. Slides for light microscopy were examined with a Nikon 80i light microscope (Nikon, Garden City, NY, U.S.A.) equipped with a Micropublisher digital camera (Q-imaging, Barnaby, British Columbia, Canada). Adobe Photoshop 7.0 (Adobe Systems Inc.) was used for adjustment of sharpness, contrast and brightness. The final images were then imported to PowerPoint software (Microsoft Windows® 2000) for assembly and labeling composite figures

Results

Western Blot characterization of α7nAChR antibody

The antibody against the α7nAChR was shown by Western blot analysis to principally recognize one immunoreactive band, in cortical tissue (Fig. 2). The α7nAChR-immunoreactive band was observed near the 50 kDa molecular weight marker in both the rat and mouse cortex. The size of this band is comparable with the molecular weight (54 kDa) of the mature, non-glycosylated α7nAChR as determined from the primary structure (Seguela et al., 1993). In the rat and mouse, the most intense immunoreactive band was observed near the 50 kDa molecular marker (Fig. 2). Compared with rat, a higher concentration of mouse cortical lysate was necessary to obtain a visible band suggesting that the α7nAChR has lower expression levels in the mouse than rat, or that the antiserum is less effective in detecting the mouse α7nAChR.

Regional and cellular distributions

By light microscopy, VAChT-immunoperoxidase labeling was localized to varicose axon-like processes found throughout the cortical lamina. In contrast, α7nAChR-immunoperoxidase

labeling was distributed in a laminar fashion and was similar in the PFC of both rat and mouse (Fig. 3). The laminar location of many labeled somata and dendrites is consistent with their identity as pyramidal neurons. The most intense α7nAChR-ir was observed in cortical layers III–V (Fig. 3B and D). The layers of the cortex were defined as in Gabbot *et al*. (1997). Punctate immunoreactivity was often seen in the perinuclear cytoplasm of these somata, but was sometimes evident in thick straight processes presumed to be dendrites that emitted from the somata. The α7nAChR-immunoperoxidase labeling also was seen in varicose axon-like processes. Omission of the primary antibody resulted in complete loss of light microscopic α7nAChR labeling in both rat and mouse PFC (not shown).

Ultrastructural analysis confirmed the presence of VAChT in axons and α7nAChR in neuronal somata as well as in dendritic and axonal processes of the PFC layer III–V. Consistent with the data from Western blots, the detected α7nAChR-immunoreactivity was more abundant in rat compared with mouse PFC. However, there was no apparent species difference in the subcellular distribution of the α7nAChR in the rat and mouse PFC. Thus, the descriptions and photographs are equally representative to both rat and mouse. The quantitative analysis was conducted exclusively in rat.

Axonal Distribution of VAChT and α7nAChR

The immunoperoxidase labeling for VAChT was seen as a dense precipitation product localized to vesicle filled axonal profiles without recognized specializations. VAChT-labeled axonal profiles were unmyelinated and 0.2– 0.7 μm in cross-sectional diameter. Many of the larger (>0.3 μm) processes contained numerous VAChT-immunoreactive small synaptic vesicles and one or more mitochondria. These axon terminals did not show recognizable specializations and were substantially less numerous than the α7nAChR-labeled profiles.

Of the total number of α7nAChR-labeled profiles in tissue processed for single and dual labeling, 24% (n = 183/771) were small axons or vesicle-filled axon terminals (Table 1). In these axonal profiles, α7nAChR labeling was observed in the cytoplasm and along the plasma membrane (Fig. 4A). The α7nAChR–labeled terminals were sometimes apposed to dendritic spines forming asymmetric synapses.

In the dual-labeling study, 47% (n = 37/79) of α7nAChR-labeled axons also contained VAChT in an area of 8,190μm^2. However, the majority (85%) of the VAChT-labeled axonal profiles were without detectable α7nAChR. Co-localization of VAChT and α7nAChR was observed in 15% (n = 37/240) of VAChT-labeled axonal processes (Fig. 4B). The α7nAChR was distributed throughout the cytoplasm and was also seen on and near the plasmalemma in VAChT-containing axonal profiles, thus suggesting the involvement of the α7nAChR in modulation of ACh release in certain axon terminals within the PFC.

Somatodendritic distribution of α7nAChR and relationship to VAChT

Somatic α7nAChR immunoperoxidase labeling was seen in punctate clusters in the cytoplasm near the nuclear membrane. Immunogold labeling for the α7nAChR was also located on cytoplasmic endomembranes and Golgi lamellae, or on the plasmalemma of many somatodendritic profiles (Fig. 4B, 5A and B). In dendritic spines, the α7nAChR immunoperoxidase labeling was localized to the thick postsynaptic densities of asymmetric, excitatory-type synapses (Fig. 6A and B). In comparison with the dense postsynaptic accumulations of immunoperoxidase, immunogold labeling for α7nAChR was sparse in postsynaptic densities, presumably because of limited penetration and lower sensitivity of immunogold as compared with immunoperoxidase labeling (Chan et al., 1990). The postsynaptic location of the α7nAChR in dendritic spines (Fig. 6A and B), and the endomembrane distributions in somata (Fig. 5B) and proximal as well as more distal dendrites

(Fig. 7A and B) are consistent with involvement of these membranes in trafficking of surface receptors (Eimer et al., 2007).

The α7nAChR-labeled somata and dendrites as well as axonal structures were observed within the same neuropil as VAChT-labeled profiles. In 4 randomly chosen 54 μm^2 square areas, from immunolabeled sections through the PFC of each rat, we observed on average 16 VAChT-labeled axons and 36 α7nAChR-labeled profiles. This suggests that ACh release from one VAChT-labeled axonal process may have access to multiple α7nACh receptors in the same or separate neurons. Of the VAChT- labeled axonal profiles observed, (99/240) were in a 4 μm radius from the nearest α7nAChR-labeled profile (Fig. 7A), with 48% of VAChT-labeled axons within a 0.2 μm radius. However, 35% (n = 35/99) of these VAChT-labeled axonal profiles were apposed to α7nAChR-labeled dendrites or somatic profiles.

Discussion

Our results provide ultrastructural evidence that in layers III–V of the PFC, α7nACh receptors are located in many postsynaptic dendrites and dendritic spines in direct contact with VAChT-containing axon terminals. Despite this proximity, the VAChT-labeled terminals do not form recognizable synapses with dendritic profiles containing α7nAChR. In addition, VAChT is expressed in 47% of α7nAChR-labeled axonal processes. Together, our results provide cellular evidence consistent with α7nAChR mediation of mainly the postsynaptic effects of ACh, but also support the involvement of these receptors in autoregulation of ACh release (Fig. 8). Both the post- and presynaptic effects mediated through α7nAChR may orchestrate cognitive functions that are dysfunctional in schizophrenic patients showing α7nAChR deficiencies (Freedman et al., 1995,Court et al., 1999).

Methodological considerations

We have shown by Western blot analysis that the α7nAChR antiserum recognizes one band in both rat and mouse cortex at approximately the molecular weight for the α7nAChR (54k DA) (Seguela et al., 1993). These results are consistent with prior reports showing the recognition of a similar molecular weight band in cultures of hippocampal neurons and in both rat and macaque brain extracts (Dominguez del Toro et al., 1994, Centeno et al., 2006, Arnaiz-Cot et al., 2008). This band is comparable to the 54–60 kDa proteins detected using α-bungarotoxin immunoprecipitation for the α7nAChR (Seguela et al., 1993, Drisdel and Green, 2000, Gotti et al., 2001). Moreover, preadsorption of the α7nAChR antibody with an antigenic blocking peptide abolishes the α7nAChR immunolabeling (Centeno et al., 2006). We also saw no α7nAChR immunoperoxidase labeling in PFC with the omission of the α7nAChR antibody in control experiments. Together these observations indicate that the α7nAChR antiserum specifically recognizes the receptor even though labeling remains in α7nAChR knockout mice (Herber et al., 2004). This conclusion is further strengthened by the facts that this antibody recognizes an α7nAChR immunoreactive band of increasing density over time in primary cultures of rat hippocampal neurons (Arnaiz-Cot *et al.*, 2008). In addition, the α7nAChR antibody used in our study has been shown to produce a similar pattern of labeling to α-bungarotoxin in the frog optic tectum (Yan et al., 2006) and the α7nAChR mRNA distribution and ligand binding in the rat central nervous system (Dominguez del Toro et al., 1994, Gotti and Clementi, 2004, Gotti et al., 2006).

Dual localization of α7nAChR and VAChT-immunolabeling was achieved by combining immunogold and immunoperoxidase pre-embedding techniques (Chan et al., 1990). However, due to the sparse distribution and limited penetration of immunogold particles, the actual number of α7nACh receptors is likely to be underestimated. In addition, the distances between profiles containing the α7nAChR and VAChT were measured in only one plane of section, which could further contribute to under-representation of those receptors that are accessible to

ACh. Profiles were considered as immunolabeled when they contained one or more gold particles or a peroxidase reaction product with an electron density greater than that seen in nearby profiles considered unlabeled. This method of quantifying profiles with one or more immunogold particles had been used previously when quantifying other receptors (Garzón and Pickel, 2006, Hara et al., 2006). However, the method is only valid when there is a minimal number of non-specific gold particles (Wang et al., 2003). All samples were selected from the tissue-plastic interface in order to minimize differences in labeling ascribed to differences in penetration of immunoreagents. In addition, the tissue was processed for immunogold labeling with the omission of the primary antisera in order to assess non-specific labeling. Gold particles were observed at the plastic surface, and these were considered as stray particles. Background labeling over myelin was not observed. In addition, the α7nAChR was most frequently observed on plasmalemmal or attached to intracellular membranes, which is consistent with the location of receptor proteins.

Axonal distribution of VAChT and α7nAChR

Consistent with previous studies (Descarries et al., 1997, Mechawar et al., 2002), VAChT-labeled axonal processes in the PFC rarely formed synapses. VAChT was co-localized with 47% of α7nAChR-labeled non-synaptic axon terminals (Fig. 8), thus providing an α7nAChR–mediated cellular substrate in the PFC for autoregulation of ACh release. This result is consistent with studies of ACh release (Araujo et al., 1988, Girod et al., 1999) and suggests that ACh is the major transmitter whose release is autoregulated through the presynaptic α7nAChR.

The presynaptic location of the α7nAChR in non-VAChT containing terminals in the PFC of rat and mouse supports the involvement of α7nAChR in areas of neurotransmission of substances other than ACh. Aspartate, dopamine, GABA, glutamate, norepinephrine and serotonin are among those transmitters whose release is increased by ACh or by α7nAChR activation (Alkondon et al., 1996, Role and Berg, 1996, Wonnacott, 1997, MacDermott et al., 1999, Schilström et al., 2000, Barik and Wonnacott, 2006, Wu et al., 2007).

Somatodendritic localization of α7nAChR and relation to VAChT

In the rat and mouse PFC, the α7nAChR was located mainly along postsynaptic densities of asymmetric axospinous synapses (Fig. 8), typical of cortical pyramidal neurons (Douglas and Martin, 1998). This observation is consistent with prior studies showing that lesions of the PFC in rat result in a 30% decrease in α-bungarotoxin binding sites in the ventral tegmental area (VTA), a major target of outputs from pyramidal neurons in the PFC (Schilström et al., 2000). Glutamate is the major neurotransmitter in PFC axon terminals that form asymmetric synapses on spiny dendrites of pyramidal neurons (Douglas and Martin, 1998). In other cortical regions, α7nACh and glutamate AMPA receptors are co-localized within dendritic spines (Levy and Aoki, 2002). Moreover, in our dual-labeling studies, none of the VAChT-labeled terminals were presynaptic to dendritic spines in which there was a postsynaptic α7nAChR distribution.

In contrast with dendritic spines, the α7nAChR in somata and dendrites had a mainly cytoplasmic distribution, associated with endomembranes (Fig. 8). In the perinuclear region of the soma, the α7nAChR was located in the Golgi lamellae and associated endomembranes. These cytoplasmic locations are consistent with assembly of the α7nAChR by the endoplasmic reticulum (Smith et al., 1987,Green and Millar, 1995) and sorting within the Golgi complex, which controls the number of cell-surface α7nAChR (Eimer et al., 2007). Endomembranes are involved in the intracellular transport of surface proteins (Gruenberg et al., 1989,Prekeris et al., 1998,Prekeris et al., 1999). Thus, the somatodendritic α7nAChR labeling may largely reflect the receptor in transit to and from the postsynaptic membrane of spiny dendrites in the

PFC. Consistent with this, the α7nAChR was only occasionally seen at the plasmalemmal surface in somata and dendrites and has been shown to be rapidly inserted and removed from the plasma membrane *via* the soluble N-ethylmaleimide-sensitive factor attachment protein receptor (SNARE) (Liu et al., 2005).

Our results are the first to show that the α7nAChR is among the ACh receptors located within somatodendritic processes that are frequently apposed to or located within a short-range (<0.2 μm) distance from ACh storage vesicles within axon terminals of the PFC (Fig. 8). This observation together with the relatively large number of α7nAChR- compared with VAChT-labeled neuronal profiles in the PFC strongly support the idea that a single cholinergic terminal in this region may influence the activity of multiple dendritic spines of the same or separate pyramidal neurons.

Implications

Our results show that in the rat and mouse PFC, the α7nAChR has a mainly postsynaptic, but also a presynaptic neuronal distribution within a functional distance of ACh vesicular storage sites. The subcellular distribution of the α7nAChR is consistent with the involvement of this receptor in modulating the postsynaptic excitability of pyramidal neurons and the axonal release of ACh in rat and mouse PFC. The results establish the functionally relevant sites for α7nAChR activation in rodent species most often used to model somatosensory gating and other deficits that are seen in schizophrenic patients lacking the α7nAChR gene (Freedman et al., 1995, Court et al., 1999, O'Neill et al., 2003).

Acknowledgments

NIH grants: HL18974, MH40342 (VMP), DA04600 (VMP), DA08259 (TAM)

We would like to thank Dr. Liping Qian for her help with the Western blot and Dr. Diane Lane for her advice on the statistical analysis.

List of Abbreviations

ACh
: Acetylcholine

α7nAChR
: Alpha-7 subunit of the nicotinic acetylcholine receptor

BSA
: Bovine serum albumin

ir
: immunoreactivity

PFC
: prefrontal cortex

PB
: phosphate buffer

PBS
: phosphate buffered saline

TBST/T
: Tris-buffered saline and Tween-20

TS

Tris-saline

VAChT

vesicular acetylcholine transporter

SNARE

N-ethylmaleimide-sensitive factor attachment protein receptor

References

Alkondon M, Rocha E, Maelicke A, Albuquerque E. Diversity of nicotinic acetylcholine receptors in rat brain. V. alpha-bungarotoxin-sensitive nicotinic receptors in olfactory bulb neurons and presynaptic modulation of glutamate release. J Pharmacol Exp Ther 1996;278:1460–1471. [PubMed: 8819534]

Araujo DM, Lapchak PA, Collier B, Quirion R. Characterization of N-[3H]methylcarbamylcholine binding sites and effect of N-methylcarbamylcholine on acetylcholine release in rat brain. J Neurochem 1988;51:292–299. [PubMed: 3379410]

Arnaiz-Cot JJ, Gonzalez JC, Sobrado M, Baldelli P, Carbone E, Gandia L, Garcia AG, Hernandez-Guijo JM. Allosteric modulation of α7 nicotinic receptors selectively depolarizes hippocampal interneurons, enhancing spontaneous GABAergic transmission. Eur J Neurosci 2008;27:1097–1110. [PubMed: 18312591]

Arvidsson U, Ried M, Elde R, Meister B. Vesicular acetylcholine transporter (VAChT) protein: A novel and unique marker for cholinergic neurons in the central and peripheral nervous systems. J Comp Neurol 1997;378:454–467. [PubMed: 9034903]

Barik J, Wonnacott S. Indirect modulation by α7 nicotinic acetylcholine receptors of noradrenaline release in rat hippocampal slices: Interaction with glutamate and GABA systems and effect of nicotine withdrawal. Mol Pharmacol 2006;69:618–628. [PubMed: 16269536]

Brunelli G, Spano P, Barlati S, Guarneri B, Barbon A, Bresciani R, Pizzi M. Glutamatergic reinnervation through peripheral nerve graft dictates assembly of glutamatergic synapses at rat skeletal muscle. Proc Natl Acad Sci U S A 2005;102:8752–8757. [PubMed: 15937120]

Butcher, L. Cholinergic neurons and networks. In: Paxinos, G., editor. The Rat Nervous System. New York: Academic Press; 1995. p. 1003-1015.

Centeno ML, Henderson JA, Pau KY, Bethea CL. Estradiol increases alpha7 nicotinic receptor in serotonergic dorsal raphe and noradrenergic locus coeruleus neurons of macaques. J Comp Neurol 2006;497:489–501. [PubMed: 16736471]

Chan J, Aoki C, Pickel VM. Optimization of differential immunogold-silver and peroxidase labeling with maintenance of ultrastructure in brain sections before plastic embedding. J Neurosci Methods 1990;33:113–127. [PubMed: 1977960]

Court J, Spurden D, Lloyd S, McKeith I, Ballard C, Cairns N, Kerwin R, Perry R, Perry E. Neuronal Nicotinic Receptors in Dementia with Lewy Bodies and Schizophrenia. J Neurochem 1999;73:1590–1597. [PubMed: 10501205]

Descarries L, Gisiger V, Steriade M. Diffuse transmission by acetylcholine in the CNS. Prog Neurobiol 1997;53:603–625. [PubMed: 9421837]

Descarries L, Mechawar N. Ultrastructural evidence for diffuse transmission by monoamine and acetylcholine neurons of the central nervous system. Prog Brain Res 2000;125:27–47. [PubMed: 11098652]

Dominguez del Toro E, Juiz JM, Peng X, Lindstrom J, Criado M. Immunocytochemical localization of the alpha 7 subunit of the nicotinic acetylcholine receptor in the rat central nervous system. J Comp Neurol 1994;349:325–342. [PubMed: 7852628]

Douglas, R.; Martin, K. Neocortex. In: Shepherd, GM., editor. The Synaptic Organization of the Brain. New York: Oxford University Press; 1998. p. 459-510.

Drisdel RC, Green WN. Neuronal alpha-bungarotoxin receptors are alpha7 Subunit Homomers. J Neurosci 2000;20:133–139. [PubMed: 10627589]

Duncan GE, Moy SS, Perez A, Eddy DM, Zinzow WM, Lieberman JA, Snouwaert JN, Koller BH. Deficits in sensorimotor gating and tests of social behavior in a genetic model of reduced NMDA receptor function. Behav Brain Res 2004;153:507–519. [PubMed: 15265649]

Eimer S, Gottschalk A, Hengartner M, Horvitz R, Richmond J, Schafer WR, Bessereau J-L. Regulation of nicotinic receptor trafficking by the transmembrane Golgi protein UNC-50. EMBO 2007;26:4313–4323.

Erickson JD, Varoqui H, Schafer MK, Modi W, Diebler MF, Weihe E, Rand J, Eiden LE, Bonner TI, Usdin TB. Functional identification of a vesicular acetylcholine transporter and its expression from a “cholinergic” gene locus. J Biol Chem 1994;269:21929–21932. [PubMed: 8071310]

Fabian-Fine R, Skehel P, Errington ML, Davies HA, Sher E, Stewart MG, Fine A. Ultrastructural Distribution of the α7 Nicotinic Acetylcholine Receptor Subunit in Rat Hippocampus. J Neurosci 2001;21:7993–8003. [PubMed: 11588172]

Freedman R, Coon H, Myles-Worsley M, Orr-Urtreger A, Olincy A, Davis A, Polymeropoulos M, Holik J, Hopkins J, Hoff M, Rosenthal J, Waldo MC, Reimherr F, Wender P, Yaw J, Young DA, Breese CR, Adams C, Patterson D, Adler LE, Kruglyak L, Leonard S, Byerley W. Linkage of a neurophysiological deficit in schizophrenia to a chromosome 15 locus. Proc Natl Acad Sci USA 1997;94:587–592. [PubMed: 9012828]

Freedman R, Hall M, Adler LE, Leonard S. Evidence in postmortem brain tissue for decreased numbers of hippocampal nicotinic receptors in schizophrenia. Biol Psychiatry 1995;38:22–33. [PubMed: 7548469]

Freedman R, Leonard S, Waldo M, Gault J, Olincy A, Adler LE. Characterization of allelic variants at chromosome 15q14 in schizophrenia. Genes, Brain and Behavior 2006;5:14–22.

Gabbott PLA, Dickie BGM, Vaid RR, Headlam AJN, Bacon SJ. Local-circuit neurones in the medial prefrontal cortex (areas 25, 32 and 24b) in the rat: Morphology and quantitative distribution 1997;377:465–499.

Garzón M, Pickel VM. Dendritic and axonal targeting of the vesicular acetylcholine transporter to membranous cytoplasmic organelles in laterodorsal and pedunculopontine tegmental nuclei. J Comp Neurol 2000;419:32–48. [PubMed: 10717638]

Garzón M, Pickel VM. Subcellular distribution of M2 muscarinic receptors in relation to dopaminergic neurons of the rat ventral tegmental area. J Comp Neurol 2006;498:821–839. [PubMed: 16927256]

Gault J, Hopkins J, Berger R, Drebing C, Logel J, Walton C, Short M, Vianzon R, Olincy A, Ross RG, Adler LE, Freedman R, Leonard S. Comparison of polymorphisms in the alpha7 nicotinic receptor gene and its partial duplication in schizophrenic and control subjects. Am J Med Genet 2003;123B:39–49. [PubMed: 14582144]

Gaykema RPA, Luiten PGM, Nyakas C, Traber J. Cortical projection patterns of the medial septum-diagonal band complex. J Comp Neurol 1990;293:103–124. [PubMed: 2312788]

Girod R, Crabtree G, Ernstrom G, Ramirez-Latorre J, McGehee D, Turner J, Role L. Heteromeric complexes of α5 and/or α7 subunits: Effects of calcium and potential role in nicotine-induced presynaptic facilitation. Ann NY Acad Sci 1999;868:578–590. [PubMed: 10414339]

Gotti C, Clementi F. Neuronal nicotinic receptors: from structure to pathology. Progress in Neurobiology 2004;74:363–396. [PubMed: 15649582]

Gotti C, Moretti M, Mantegazza R, Fornasari D, Tsouloufis T, Clementi F. Antineuronal nicotinic receptor antibodies in MG patients with thymoma. J Neuroimmunol 2001;113:142–145. [PubMed: 11137585]

Gotti C, Zoli M, Clementi F. Brain nicotinic acetylcholine receptors: native subtypes and their relevance. Trends in Pharmacological Sciences 2006;27:482–491. [PubMed: 16876883]

Green WN, Millar NS. Ion-channel assembly. Trends in Neurosciences 1995;18:280–287. [PubMed: 7571003]

Gruenberg J, Griffiths G, Howell KE. Characterization of the early endosome and putative endocytic carrier vesicles in vivo and with an assay of vesicle fusion in vitro. J Cell Biol 1989;108:1301–1316. [PubMed: 2538480]

Guan ZZ, Zhang X, Blennow K, Nordberg A. Decreased protein level of nicotinic receptor α7 subunit in the frontal cortex from schizophrenic brain. Neuroreport 1999;10:1779–1782. [PubMed: 10501574]

Hara Y, Pickel VM. Preferential relocation of the N-methyl-d-aspartate receptor NR1 subunit in nucleus accumbens neurons that contain dopamine D1 receptors in rats showing an apomorphine-induced sensorimotor gating deficit. Neurosci 2008;154:965–977.

Hara Y, Yakovleva T, Bakalkin G, Pickel VM. Dopamine D1 receptors have subcellular distributions conducive to interactions with prodynorphin in the rat nucleus accumbens shell. Synapse 2006;60:1–19. [PubMed: 16575853]

Henny P, Jones BE. Projections from basal forebrain to prefrontal cortex comprise cholinergic, GABAergic and glutamatergic inputs to pyramidal cells or interneurons. Eur J Neurosci 2008;27:654–670. [PubMed: 18279318]

Herber DL, Severance EG, Cuevas J, Morgan D, Gordon MN. Biochemical and Histochemical Evidence of Nonspecific Binding of α7nAChR Antibodies to Mouse Brain Tissue. J Histochem Cytochem 2004;52:1367–1376. [PubMed: 15385583]

Hsu SM, Raine L, Fanger H. Use of avidin-biotin-peroxidase complex (ABC) in immunoperoxidase techniques: a comparison between ABC and unlabeled antibody (PAP) procedures. J Histochem Cytochem 1981;29:577–580. [PubMed: 6166661]

Kaplan TJ, Skyers PR, Tabori NE, Drake CT, Milner TA. Ultrastructural evidence for mu-opioid modulation of cholinergic pathways in rat dentate gyrus. Brain Res 2004;1019:28–38. [PubMed: 15306235]

Lane DA, Lessard AA, Chan J, Colago EEO, Zhou Y, Schlussman SD, Kreek MJ, Pickel VM. Region-specific changes in the subcellular distribution of AMPA receptor GluR1 subunit in the rat ventral tegmental area after acute or chronic morphine administration. J Neurosci 2008;28:9670–9681. [PubMed: 18815253]

Lehmann J, Nagy JI, Atmadja S, Fibiger HC. The nucleus basalis magnocellularis: The origin of a cholinergic projection to the neocortex of the rat. Neuroscience 1980;5:1161–1174. [PubMed: 7402465]

Leonard S, Gault J, Hopkins J, Logel J, Vianzon R, Short M, Drebing C, Berger R, Venn D, Sirota P, Zerbe G, Olincy A, Ross RG, Adler LE, Freedman R. Association of Promoter Variants in the α7 Nicotinic Acetylcholine Receptor Subunit Gene With an Inhibitory Deficit Found in Schizophrenia. Arch Gen Psychiatry 2002;59:1085–1096. [PubMed: 12470124]

Levy RB, Aoki C. Alpha 7 nicotinic acetylcholine receptors occur at postsynaptic densities of AMPA receptor-positive and -negative excitatory synapses in rat sensory cortex. J Neurosci 2002;22:5001–5015. [PubMed: 12077196]

Liu Z, Tearle AW, Nai Q, Berg DK. Rapid activity-driven SNARE-dependent trafficking of nicotinic receptors on somatic spines. J Neurosci 2005;25:1159–1168. [PubMed: 15689552]

Lubin M, Erisir A, Aoki C. Ultrastructural immunolocalization of the α7 nAChR subunit in guinea pig medial prefrontal cortex. Ann NY Acad Sci 1999;868:628–632. [PubMed: 10414345]

MacDermott AB, Role LW, Siegelbaum SA. Presynaptic ionotrophic receptors and the control of transmitter release. Annu Rev Neurosci 1999;22:443–485. [PubMed: 10202545]

Martin-Ruiz CM, Haroutunian VH, Long P, Young AH, Davis KL, Perry EK, Court JA. Dementia rating and nicotinic receptor expression in the prefrontal cortex in schizophrenia. Biol Psychiatry 2003;54:1222–1233. [PubMed: 14643090]

Martin LF, Kem WR, Freedman R. Alpha-7 nicotinic receptor agonists: potential new candidates for the treatment of schizophrenia. Psychopharmacology (Berl) 2004;174:54–64. [PubMed: 15205879]

Marutle A, Zhang X, Court J, Piggott M, Johnson M, Perry R, Perry E, Nordberg A. Laminar distribution of nicotinic receptor subtypes in cortical regions in schizophrenia. J Chem Neuroanat 2001;22:115–126. [PubMed: 11470559]

McLane KE, Wu X, Lindstrom JM, Conti-Tronconi BM. Epitope mapping of polyclonal and monoclonal antibodies against two alpha-bungarotoxin-binding alpha subunits from neuronal nicotinic receptors. J Neuroimmunlo 1992;38:115–128.

Mechawar N, Watkins KC, Descarries L. Ultrastructural features of the acetylcholine innervation in the developing parietal cortex of rat. J Comp Neurol 2002;443:250–258. [PubMed: 11807835]

O'Neill H, Rieger K, Kem W, Stevens K. DMXB, an α7 nicotinic agonist, normalizes auditory gating in isolation-reared rats. Psychopharmacology 2003;169:332–339. [PubMed: 12759805]

Paxinos, G.; Franklin, KBJ. The Mouse Brain in Stereotaxic Coordinates. San Diego: Academic Press; 2001.

Paxinos, G.; Watson, C. The rat brain in stereotaxic coordinates. Orlando: Academic Press; 1986.

Peters, A.; Palay, SL.; Webster, HD. The fine structure of the nervous system. New York: Oxford University Press; 1991.

Pickel VM, Douglas J, Chan J, Gamp PD, Bunnett NW. Neurokinin 1 receptor distribution in cholinergic neurons and targets of substance P terminals in the rat nucleus accumbens. J Comp Neurol 2000;423:500–511. [PubMed: 10870089]

Prekeris R, Foletti DL, Scheller RH. Dynamics of Tubulovesicular Recycling Endosomes in Hippocampal Neurons. J Neurosci 1999;19:10324–10337. [PubMed: 10575030]

Prekeris R, Klumperman J, Chen YA, Scheller RH. Syntaxin 13 Mediates Cycling of Plasma Membrane Proteins via Tubulovesicular Recycling Endosomes. J Cell Biol 1998;143:957–971. [PubMed: 9817754]

Reynolds ES. The use of lead citrate at high pH as an electron-opaque stain in electron microscopy. J Cell Biol 1963;17:208–212. [PubMed: 13986422]

Roghani A, Feldman J, Kohan SA, Shirzadi A, Gundersen CB, Brecha N, Edwards RH. Molecular cloning of a putative vesicular transporter for acetylcholine. Proc Natl Acad Sci USA 1994;91:10620–10624. [PubMed: 7938002]

Role LW, Berg DK. Nicotinic receptors in the development and modulation of CNS synapses. Neuron 1996;16:1077–1085. [PubMed: 8663984]

Schilström B, Fagerquist MV, Zhang X, Hertel P, Panagis G, Nomikos GG, Svensson TH. Putative role of presynaptic alpha7 nicotinic receptors in nicotine stimulated increases of extracellular levels of glutamate and aspartate in the ventral tegmental area. Synapse 2000;38:375–383. [PubMed: 11044884]

Schoepfer R, Conroy WG, Whiting P, Gore M, Lindstrom J. Brain α-bungarotoxin binding protein cDNAs and MAbs reveal subtypes of this branch of the ligand-gated ion channel gene superfamily. Neuron 1990;5:35–48. [PubMed: 2369519]

Seguela P, Wadiche J, Dineley-Miller K, Dani JA, Patrick JW. Molecular cloning, functional properties, and distribution of rat brain alpha 7: a nicotinic cation channel highly permeable to calcium. J Neurosci 1993;13:596–604. [PubMed: 7678857]

Severance EG, Yolken RH. Novel Alpha-7 nicotinic receptor isoforms and deficient cholinergic transcription in schizophrenia. Genes Brain Behav 2008;7:37–45. [PubMed: 17504249]

Smith MM, Lindstrom J, Merlie JP. Formation of the alpha-bungarotoxin binding site and assembly of the nicotinic acetylcholine receptor subunits occur in the endoplasmic reticulum [published erratum appears in J Biol Chem 1987 Jul 5;262(19):9428]. J Biol Chem 1987;262:4367–4376. [PubMed: 3549731]

Svingos AL, Colago EE, Pickel VM. Vesicular acetylcholine transporter in the rat nucleus accumbens shell: Subcellular distribution and association with mu-opioid receptors. Synapse 2001;40:184–192. [PubMed: 11304756]

Towart LA, Alves SE, Znamensky V, Hayashi S, McEwen BS, Milner TA. Subcellular relationships between cholinergic terminals and estrogen receptor-α in the dorsal hippocampus. J Comp Neurol 2003;463:390–401. [PubMed: 12836175]

Wang H, Cuzon VC, Pickel VM. Postnatal development of [mu]-opioid receptors in the rat caudate-putamen nucleus parallels asymmetric synapse formation. Neuroscience 2003;118:695–708. [PubMed: 12710977]

Wonnacott S. Presynaptic nicotinic ACh receptors. Trends Neurosci 1997;20:92–98. [PubMed: 9023878]

Woolf NJ. Cholinergic systems in mammalian brain and spinal cord. Prog Neurobiol 1991;37:475–524. [PubMed: 1763188]

Wu J, Khan GM, Nichols RA. Dopamine release in prefrontal cortex in response to β-amyloid activation of α7 nicotinic receptors. Brain Res 2007;1182:82–89. [PubMed: 17935702]

Yan X, Zhao B, Butt CM, Debski EA. Nicotine exposure refines visual map topography through an NMDA receptor-mediated pathway 2006;24:3026–3042.

Zaborszky L, Gaykema RP, Swanson DJ, Cullinan WE. Cortical input to the basal forebrain. Neuroscience 1997;79:1051–1078. [PubMed: 9219967]

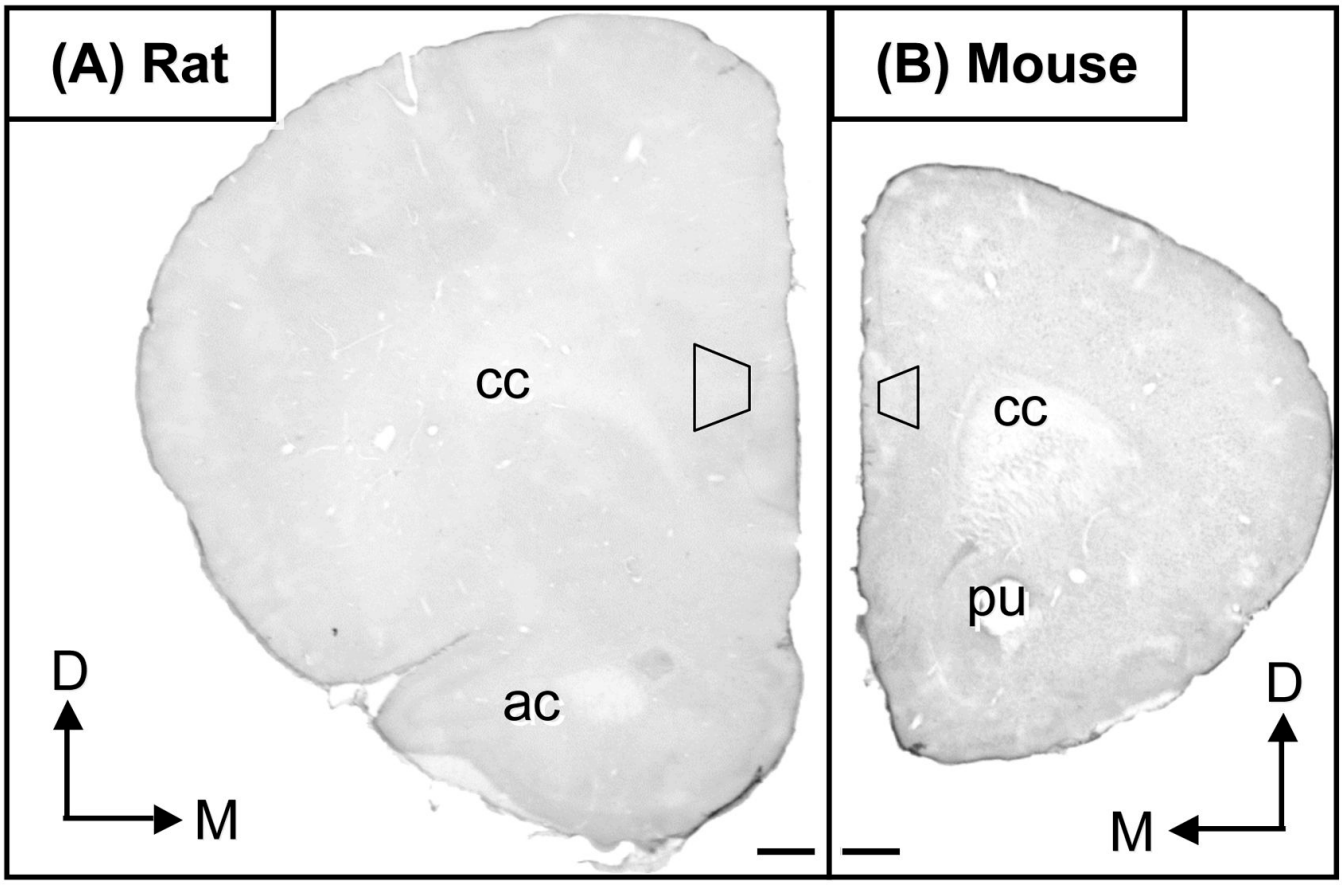

Fig. 1.

Light micrographs showing coronal hemisections through (A) rat and (B) mouse PFC. These sections were cut with a vibratome at rostrocaudal levels defined anterior to Bregma as +2.80 mm in rat (Paxinos and Watson, 1986) and +2.20 mm in mouse (Paxinos and Franklin, 2001) from the mouse. The tissue was processed for immunoperoxidase labeling of the α7nAChR. The trapezoids show the portion of the PFC that was sampled for electron microscopy. Arrows indicate the dorsal (D) and medial (M) brain surfaces. ac = anterior commissure, cc = corpus callosum, pu = identifying hole punched in mouse. Scale bars = 500 μm.

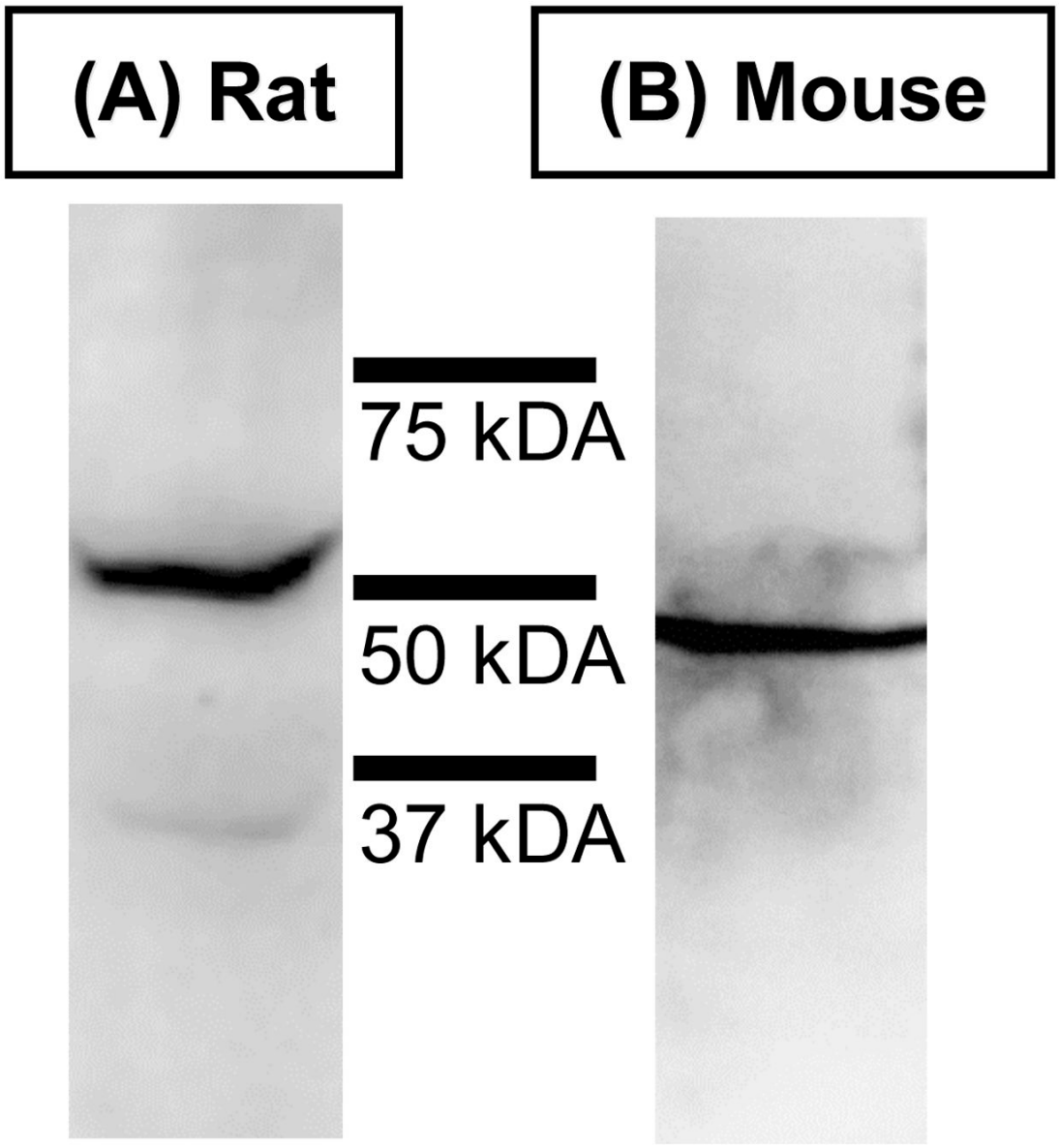

Fig. 2.

Western blots for characterization of the antibody against the α7nAChR using cortical protein lysates from (A) rat and (B) mouse. A single dominant band is detected in both the rat and mouse near the 50 kDa molecular weight marker which is comparable with the 54 kDa molecular weight of the α7nAChR (Seguela et al., 1993) indicating the specificity of the antibody to the α7nAChR.

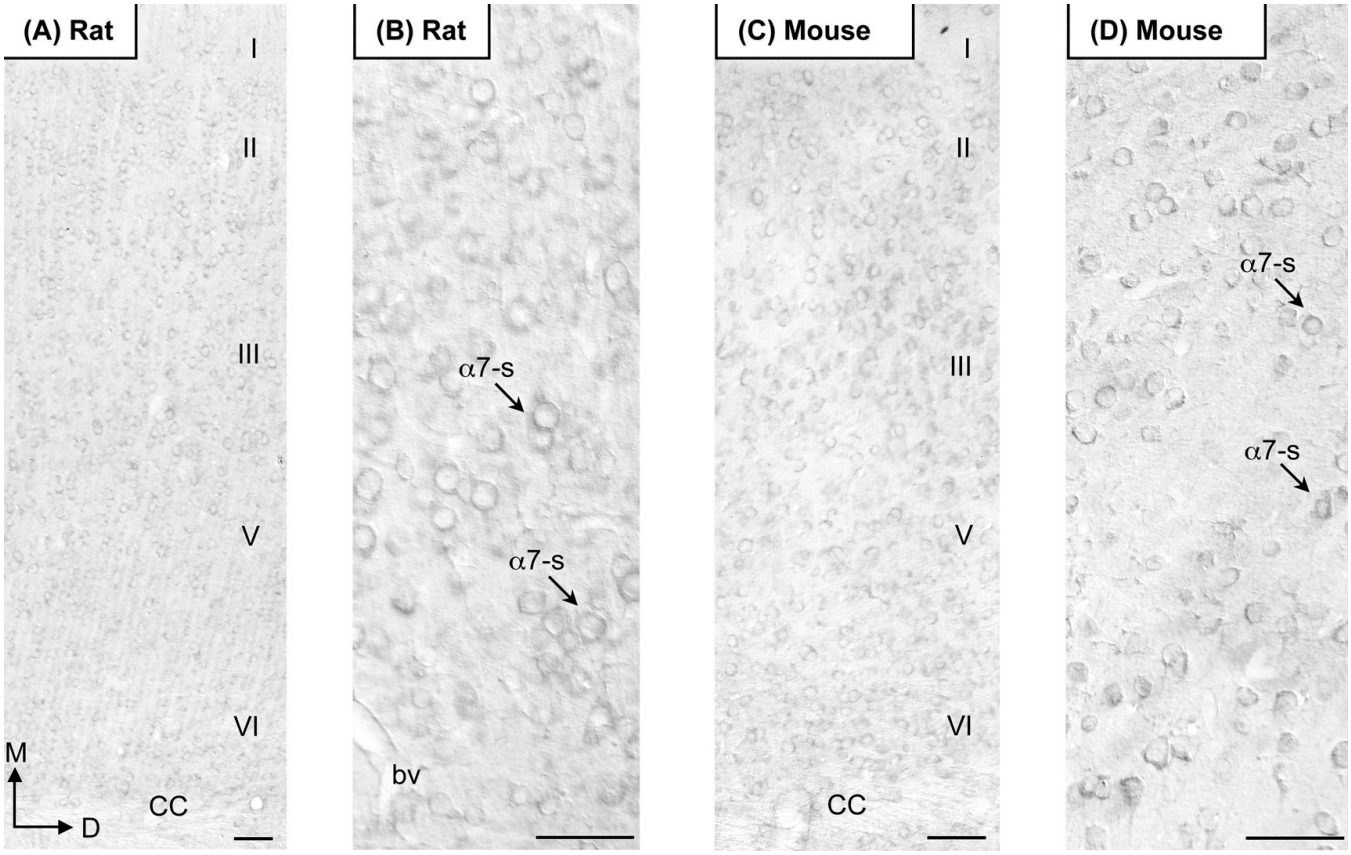

Fig. 3.

Light micrographs showing the regional distribution of immunoperoxidase labeling for the α7nAChR in coronal sections through the PFC in the (A and B) rat (+2.8 mm from Bregma) and (C and D) mouse (+2.2 mm from Bregma). The α7nAChR labeling is seen in cells throughout layers I–VI of the PFC. The majority of the somatic α7nAChR labeling (α7-s) is in layer III–V, the area sampled for electron microscopic analysis and enlarged in (B) and (D). Arrows indicate the dorsal (D) and medial (M) brain surfaces. bv = blood vessel, cc = corpus callosum. Scale bars = 50 μm.

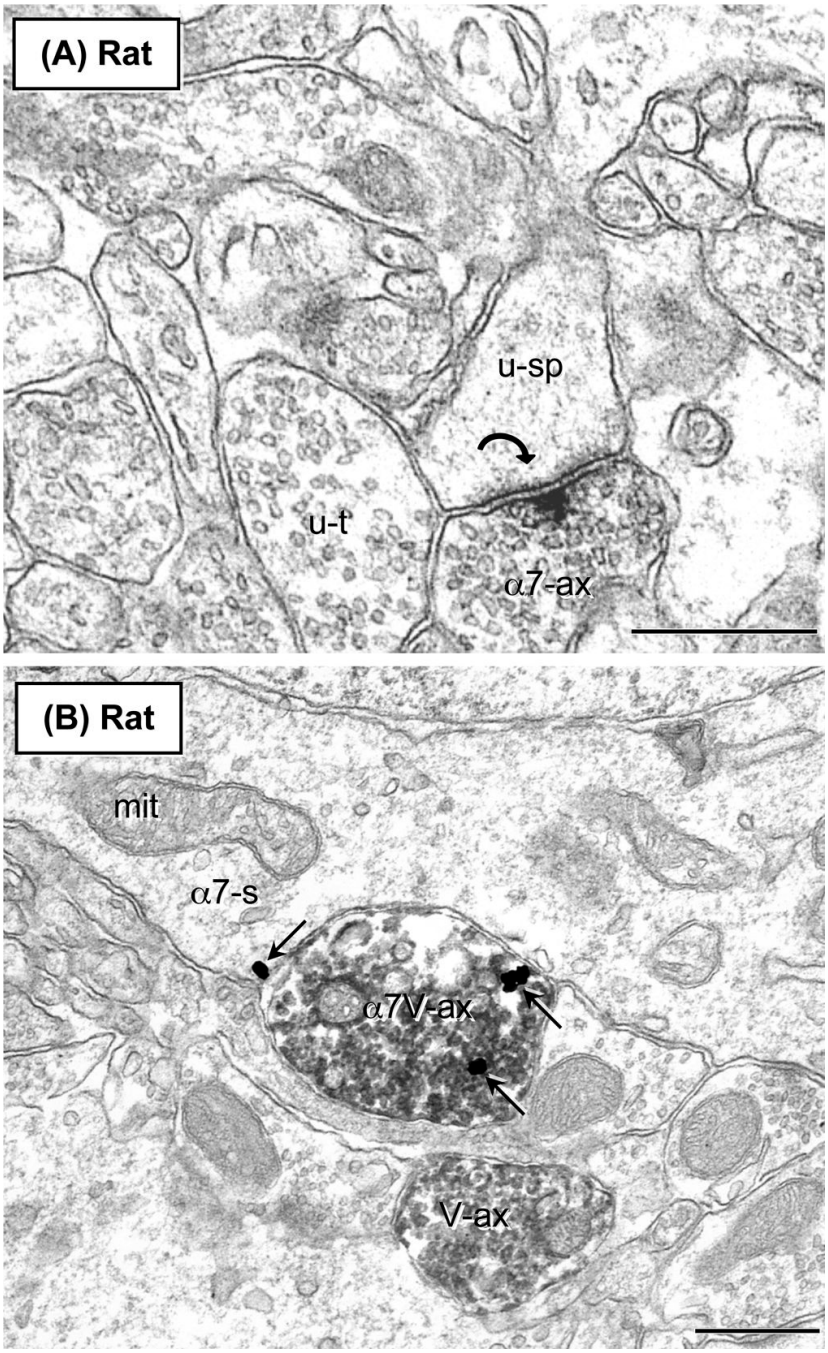

Fig. 4.

Electron micrographs showing the presynaptic location of the α7nAChR and VAChT in (A) single-labeled and (B) dual-labeled rat PFC. (A) Immunoperoxidase labeling (block arrow) of the α7nAChR is seen along the presynaptic membrane of an axon terminal (α7-ax) forming an asymmetric synapse (curved arrow) with an unlabeled dendritic spine (u-sp). (B) Immunoperoxidase labeling for the VAChT in vesicle filled axonal profiles, one of which shows immunogold labeling (small arrows) for the α7nAChR (α7V-ax). This terminal is apposed to a somata (α7-s) showing a single immunogold particle on the plasma membrane in contact with the dual-labeled terminal. u-t = unlabeled terminal. Scale bars = 500 nm.

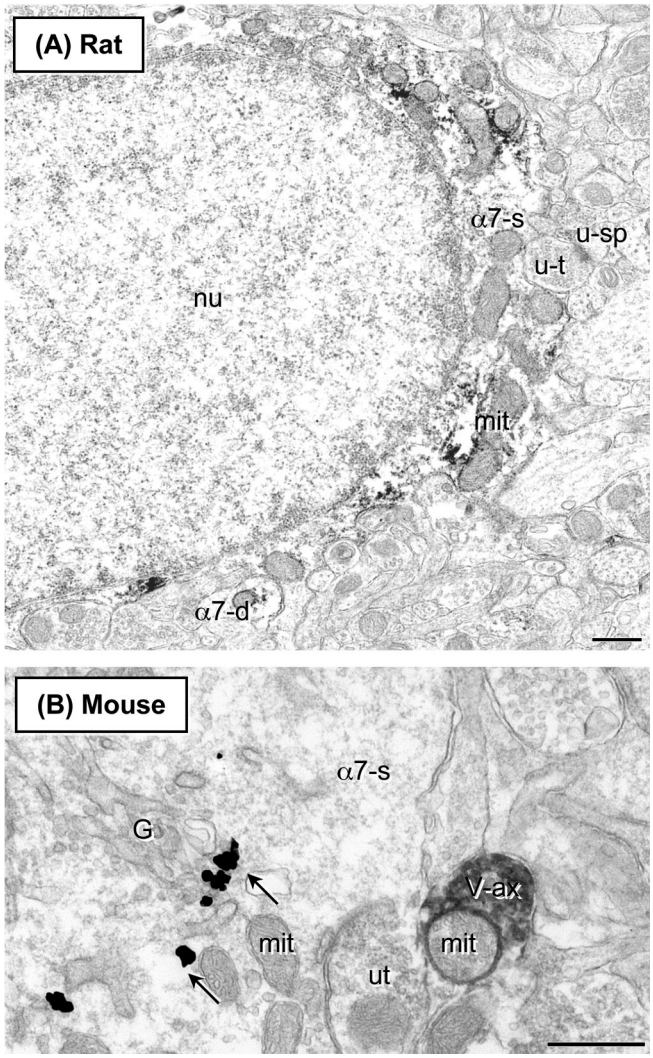

Fig. 5.

Electron microscopic immunoperoxidase and immunogold labeling for the α7nAChR in the cytoplasm of neuronal somata (α7-s) in (A) single-labeled rat and (B) dual-labeled mouse PFC. (A) The α7nAChR immunoperoxidase labeling is in the perinuclear cytoplasm of the soma (α7-s). A α7nAChR-labeled dendrite (α7-d) is also seen within the adjacent neuropil. (B) Immunogold labeling of the α7nAChR has a prominent location in the perinuclear cytoplasm, where the immunogold particles are associated with outer Golgi lamella (G). Immunoperoxidase-labeling for VAChT is in an axonal profile (V-ax) apposing the α7-s. mit = mitochondria, nu = nucleus, u-sp = unlabeled spine, u-t = unlabeled terminal. Scale bars = 500 nm.

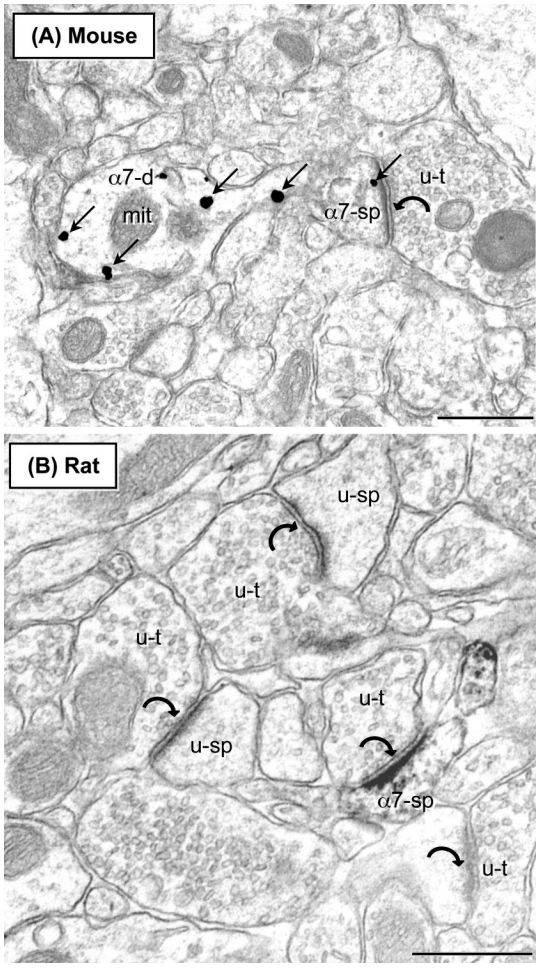

Fig. 6.

Single immunogold (A) and immunoperoxidase labeling (B) of the α7nAChR in dendritic spines in electron micrographs from mouse and rat PFC (A and B, respectively). (A) An α7nAChR-labeled dendrite (α7-d) with a spine (α7-sp) that has a single gold particle (small arrows) identifying α7nAChR. The spine receives an asymmetric synapse (curved arrow) from an unlabeled axon terminal (u-t). The peroxidase density can be compared with that seen in other spines that are unlabeled (u-sp) and also received asymmetric synapses from unlabeled terminals. (u-t). Scale bars = 500 nm.

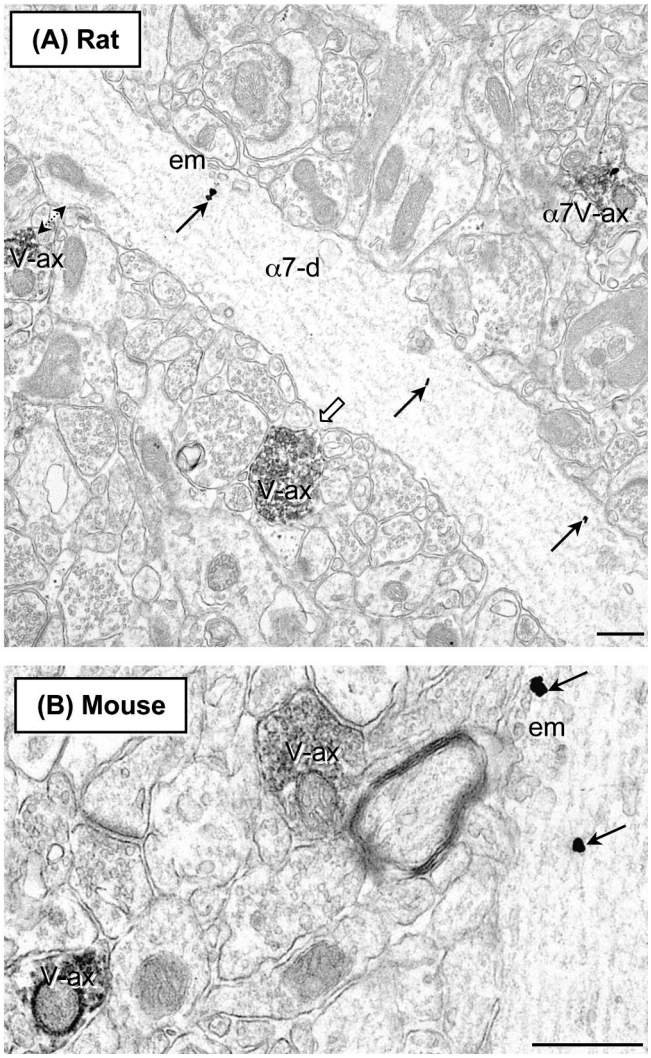

Fig. 7.

Dendritic distribution of α7nAChR immunogold labeling in relation to axon terminals containing the VAChT as seen by dense immunoperoxidase reaction product in rat (A) and mouse (B) PFC. (A) A large longitudinally oriented dendrite with cytoplasmic α7nAChR immunogold labeling (α7-d, black arrows), is seen in contact with a VAChT-labeled axon (V-ax; white arrow), < 0.2 μm (double head arrow) from a V-ax and third V-ax is > 0.2 μm from the α7-d. In the (B) mouse, longitudinally orientated α7-d, in which the immunogold particles are associated with endomembranes (em) near a VAChT-immunoperoxidase labeled axon terminal (V-ax). Scale bars = 500 nm.

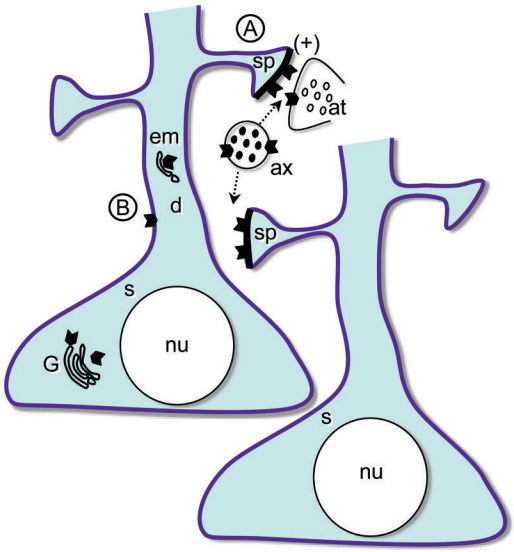

Fig. 8.

Schematic diagram showing the subcellular distributions of the α7nAChR in relation to the VAChT in the rodent prefrontal cortex (PFC). (A) The α7nAChR (black chevrons) is shown as having a presynaptic distribution in axon terminals (at), forming excitatory (+) axospinous synapses and co-localized in VAChT-labeled (black circles) axonal processes, in the vicinity of α7nAChR-labeled spines (sp). (B) The α7nAChR has a somatodendritic distribution in dendrites (d) and somata (s), where it is attached to endomembranes (em), Golgi lamella (G) and on plasmalemmal membrane (purple line) of spiny neurons (light blue). nu = nucleus.

Tabel I

Subcellular distribution of α7nAChR and VACHT in the PFC

Neuronal Profiles	* **Single- α7nAChR labeled tissue**		** **Dual-α7nAChR/VAChT labeled tissue**	
α7nAChR	*Percentage*	*(number)*	*Percentage*	*(number)*
Axons	23	(104)	25	(79)
Spines	34	(159)	35	(107)
Dendrites	30	(140)	26	(88)
Somata	13	(60)	11	(34)
Total	100	463	100	308
VAChT				
Axons			99	(203)
Spines			0.5	(1)
Dendrites			0.5	(1)
Total			100	205
α7nAChR/VAChT				
Axons			97.4	(37)
Somata			2.6	(1)
Total			100	38

*Single-labeling: 9,799 μm^2 tissue

**Dual-labeling: 8,190 μm^2 tissue